Acta Oceanol. Sin., 2019, Vol. 38, No. 3, P. 45–59
https://doi.org/10.1007/s13131-019-1398-2
http://www.hyxb.org.cn
E-mail: hyxbe@263.net

Wave packet solutions in a bounded equatorial ocean and its interannual and decadal variabilities

Dongling Zhang[1], Juan Zhu[2, 3], Xu Lu[3, 4], Ming Zhang[3]*

[1] Institute of Atmospheric Physics, Chinese Academy of Sciences, Beijing 100029, China

[2] Special Office of Marine Environment, National Marine Environment Forecasting Center, Ministry of Natural Resources, Beijing 100081, China

[3] Atmospheric Circulation and Short-term Climate Prediction Laboratory of Meteorology and Marine Institute, National University of Defense Technology, Nanjing 211101, China

[4] 32021 Troop, People's Liberation Army, Beijing 100094, China

Received 25 January 2018; accepted 6 March 2018

Abstract

Linearized shallow water perturbation equations with approximation in an equatorial β plane are used to obtain the analytical solution of wave packet anomalies in the upper bounded equatorial ocean. The main results are as follows. The wave packet is a superposition of eastward travelling Kelvin waves and westward travelling Rossby waves with the slowest speed, and satisfies the boundary conditions of eastern and western coasts, respectively. The decay coefficient of this solution to the north and south sides of the equator is inversely proportional only to the phase velocity of Kelvin waves in the upper water. The oscillation frequency of the wave packet, which is also the natural frequency of the ocean, is proportional to its mode number and the phase velocity of Kelvin waves and is inversely proportional to the length of the equatorial ocean in the east-west direction. The flow anomalies of the wave packet of Mode 1 most of the time appear as zonal flows with the same direction. They reach the maximum at the center of the equatorial ocean and decay rapidly away from the equator, manifested as equatorially trapped waves. The flow anomalies of the wave packet of Mode 2 appear as the zonal flows with the same direction most of the time in half of the ocean, and are always 0 at the center of the entire ocean which indicates stagnation, while decaying away from the equator with the same speed as that of Mode 1. The spatial structure and oscillation period of the wave packet solution of Mode 1 and Mode 2 are consistent with the changing periods of the surface spatial field and time coefficient of the first and second modes of complex empirical orthogonal function (EOF) analysis of flow anomalies in the actual equatorial ocean. This indicates that the solution does exist in the real ocean, and that El Niño-Southern Oscillation (ENSO) and Indian Ocean dipole (IOD) are both related to Mode 2. After considering the Indonesian throughflow, we can obtain the length of bounded equatorial ocean by taking the sum of that of the tropical Indian Ocean and the tropical Pacific Ocean, thus this wave packet can also explain the decadal variability (about 20 a) of the equatorial Pacific and Indian Oceans.

Key words: bounded equatorial ocean, wave packet solutions, decadal variability, Kelvin wave, Rossby wave

Citation: Zhang Dongling, Zhu Juan, Lu Xu, Zhang Ming. 2019. Wave packet solutions in a bounded equatorial ocean and its interannual and decadal variabilities. Acta Oceanologica Sinica, 38(3): 45–59, doi: 10.1007/s13131-019-1398-2

1 Introduction

The earliest research of an equatorial wave system was done by Matsuno (1966). As the Coriolis parameter f is 0 and its derivative $\beta = \mathrm{d}f/\mathrm{d}y$ reaches a maximum at the equator, fluctuations in equatorial waters become the most distinctive motion in marine dynamics. In the equatorial ocean, there are Kelvin waves travelling eastward and Rossby waves travelling westward, as well as inertial gravity waves of high frequency and mixed Rossby inertial-gravity waves. These waves constitute the Matsuno wave system, also known as the equatorial wave system. The adjustment of Kelvin and Rossby waves in the equatorial wave system will produce the oscillation of the interannual time scale and can explain El Niño-Southern Oscillation (ENSO) circulation. Thus, the importance of the fluctuations in the equatorial waters has gradually been recognized.

Waves which propagate in parallel with the shoreline but become obvious only in the vicinity of the shoreline were first studied by Lord Kelvin and are thus named after their discoverer. Obviously the constraint of shoreline is an important factor. Matsuno (1966) found that similar waves also exist even without the constraint of shoreline when the Coriolis parameter changes with space, a condition in which a wave form is only obvious close to the equator and there is only one eastward moving wave. Here, the equator plays the role of shoreline. Hirst (1989) and Yamagata and Masumoto (1989) theoretically proved that disturbances propagating to the east exist in an ocean-atmosphere coupled model, which they believe is induced by eastward moving equatorial Kelvin waves. We also found that subsurface ocean temperature anomalies (SOTA) in the tropical Pacific propagate from west to east along the thermocline of the equator in years of both higher-than-average plum rain precipitation and lower-than-av-

Foundation item: The National Major Research High Performance Computing Program of China under contract 2016YFB0200800; the Strategic Priority Research Program of Chinese Academy of Sciences under contract No. XDA20060501.
*Corresponding author, E-mail: zhangm1945@163.com

erage plum rain precipitation in the middle and lower reaches of the Changjiang (Yangtze) River (Lu and Zhang, 2009), which suggests that this may be related with eastward moving Kelvin waves in the equatorial Pacific.

Nevertheless, as there are coastlines in the eastern and western tropical Pacific, Kelvin waves will inevitably be reflected by the eastern boundaries of the ocean as they travel eastward, disrupting their mode of propagation, which has been used to explain the ENSO (Chao, 1993). This indicates that travelling Kelvin waves in an equatorial ocean cannot satisfy lateral boundary conditions from the perspective of mathematical physics, nor is it the solution of that bounded ocean. All of the three major tropical oceans, i.e., the Pacific, the Indian Ocean and the Atlantic Ocean, have boundaries. Thus it is of great significance to seek the solution of equatorial oceans with boundaries in the equator wave system. Does the solution exist? If it does, what are its spatial structure and vibrational frequencies? How is it connected with climate change? These are key issues of physical oceanography and climate science. Existing research in this regard, however, is lacking, and the above questions remain largely unanswered. Our earlier analyses (Zhang, 2006; Zhang and He, 2005; Lu et al., 2014) of complex EOF (empirical orthogonal function) for the flow field anomalies of the tropical Pacific and the tropical Indian Ocean show that the spatial field of anomalous flow fields, in the form of zonal flows, is trapped near the equator and decays rapidly away from it. This suggests that these equatorial flow field anomalies are very likely to be a wave packet solution satisfying the requirement of the wave system of bounded equatorial oceans. This wave packet solution may play an important role in the flow field anomalies in the equatorial ocean. An ideal ocean model is used in this paper to answer these questions and prove the above hypothesis that the mode of the complex EOF for the flow field anomalies is the wave packet solution of the bounded equatorial oceans. Since the upper ocean above the thermocline can be seen as positive, linearized shallow disturbance equations (positive) with approximation in the equatorial β plane is used in this paper. By introducing reduced gravity (Zhang, 1995) and taking the lateral boundary conditions of the east and west coasts in an ideal ocean into account, the paper seeks the analytical solution of wave packet perturbation (anomaly) of the bounded ocean in a climatic scale, which is necessary and highly significant for understanding its shape and characteristics and for explaining the nature of the complex EOF analysis results of the flow field anomalies made earlier on the tropical Pacific and Indian Oceans.

2 Mathematical model and its solution

Suppose the ocean is divided homogeneously in the vertical direction into upper and lower layers, which is bounded by thermocline. The densities of the two layers are constant ρ_1 and ρ_2 respectively after the introduction of reduced gravity (Zhang and He, 2005). Suppose the lower ocean is still, then the governing equation of the upper ocean may be considered as satisfying linearized shallow disturbance equations (positive) with approximation in equatorial the β plane.

$$\frac{\partial u}{\partial t} - \beta y v = -\hat{g}\frac{\partial \eta}{\partial x}, \tag{1a}$$

$$\frac{\partial v}{\partial t} + \beta y u = -\hat{g}\frac{\partial \eta}{\partial y}, \tag{1b}$$

$$\frac{\partial \eta}{\partial t} + \bar{H}\left(\frac{\partial u}{\partial x} + \frac{\partial v}{\partial y}\right) = 0, \tag{1c}$$

where $\bar{H}$ is the average depth of the upper layer and is a constant; η represents a small disturbance near $\bar{H}$; $\hat{g} = (\rho_2 - \rho_1)\, g/\rho_2$, is reduced gravity and $g$is the gravity. In the non-dimensionalization of the above equations, "′" represents the non-dimensional variables. $u' = u/\bar{U}$, $v' = v/\bar{V}$ and $\delta\eta' = \Delta\eta/\Delta\bar{\eta}$, are introduced for dependent variables, with "-" representing the corresponding scale. $x' = x/L_x$, $y' = y/L_y$ and $t' = t/\bar{t}$ are introduced for independent variables. Here L_x, L_y and $\bar{t}$ represent the scale of corresponding variables. Then the corresponding dimensionless equations (Xuan et al., 2014; Wu, 2002) can be obtained as follows:

$$\frac{\partial u}{\partial t} - yv = -\frac{\partial \eta}{\partial x}, \tag{2a}$$

$$\varepsilon\frac{\partial v}{\partial t} + yu = -\frac{\partial \eta}{\partial y}, \tag{2b}$$

$$\frac{\partial \eta}{\partial t} + \frac{\partial u}{\partial x} + \frac{\partial v}{\partial y} = 0, \tag{2c}$$

where $\varepsilon = L_y/L_x$ and it is equivalent to long wave approximation when $\varepsilon = 0$. The symbol "′" representing non-dimensional variables in Eq. (2) is omitted for the convenience of writing and so is in the following text unless otherwise indicated. Suppose the wave solution is

$$(u, v, \eta)^{\mathrm{T}} = [U(y), \mathrm{i}V(v), \Phi(y)]^{\mathrm{T}} \cdot \mathrm{e}^{i(kx-\omega t)}, \tag{3}$$

where Φ represents the structure of η in the y (meridional) direction.

Then

$$\omega U + yV = k\Phi, \tag{4a}$$

$$\varepsilon\omega V + yU = -\frac{\mathrm{d}\Phi}{\mathrm{d}y}, \tag{4b}$$

$$-\omega\Phi + kU + \frac{\mathrm{d}V}{\mathrm{d}y} = 0. \tag{4c}$$

The solution of Eq. (4) is as follows. First considering the simplest Kelvin wave, we set $V \equiv 0$. Thus, according to the existing literature (Xuan et al., 2014; Wu, 2002), the dispersion relation of ω and $k$can be obtained as

$$\omega = k. \tag{5}$$

It can be seen that the wave propagates eastward, and the solution of the wave is

$$U = \tilde{U}\mathrm{e}^{-\frac{\omega}{2k}y^2} = \tilde{U}\mathrm{e}^{-\frac{1}{2}y^2}, \tag{6a}$$

$$\Phi = \frac{\omega}{k}U = \tilde{U}\frac{\omega}{k}\mathrm{e}^{-\frac{\omega}{2k}y^2} = \tilde{\Phi}\mathrm{e}^{-\frac{1}{2}y^2}, \tag{6b}$$

where $\tilde{U}$ is a random integral constant; and $\tilde{\Phi} = \tilde{U}\omega/k$, is the amplitude of Kelvin wave.

Next, we take general circumstances into account. According

to literature (Xuan et al., 2014; Wu, 2002), similarly, by eliminating U and Φ from Eq. (4), we can get the second-order linear equation with variable coefficients as

$$\frac{\mathrm{d}^2V}{\mathrm{d}y^2}+\left[\varepsilon\left(\omega^2-k^2\right)-\frac{k}{\omega}-y^2\right]V=0. \tag{7}$$

This is a Hermite equation, which means its solution with boundaries, i.e., the solution with physical significance, contains Hermite polynomials. This solution must satisfy the following condition (Wu, 2002; Zhang and Zhang, 2006):

$$\varepsilon\left(\omega^2-k^2\right)-\frac{k}{\omega}=2n+1\ ,\quad n=0,\ 1,\ 2,\ \cdots, \tag{8}$$

The above formula is also the dispersion relation of ω and k. The solution meeting the requirement of this dispersion relation is

$$V=\hat{V}\cdot \mathrm{H}_n(y)\cdot \mathrm{e}^{-\frac{1}{2}y^2}, \tag{9a}$$

were $\hat{V}$ is also a random integral constant and $\mathrm{H}_n(y)$ are Hermite polynomials. The first six polynomials are $\mathrm{H}_0(y)=1$, $\mathrm{H}_1(y)=2y$, $\mathrm{H}_2(y)=4y^2-2$, $\mathrm{H}_3(y)=2^3y^3-12y$, $\mathrm{H}_4(y)=2^4y^4-48y^2+12$, $\mathrm{H}_5(y)=2^5y^5-160y^3+120y$, respectively. By eliminating Φ from Eq. (4), we can get $\left(\omega^2-k^2\right)U+\omega yV-k\mathrm{d}V/\mathrm{d}y=0$. By substituting Eq. (9a) in this equation and using derivative formula of Hermite polynomials $\mathrm{dH}_n/\mathrm{d}y=2n\mathrm{H}_{n-1}$ and recursive formula $\mathrm{H}_{n+1}=2y\mathrm{H}_n-2n\mathrm{H}_{n-1}$, we can get the following equation:

$$U=\hat{U}\left[-\frac{k\mathrm{H}_{n+1}(y)}{\omega^2-k^2}+(k+\omega)\,y\mathrm{H}_n(y)\right]\mathrm{e}^{-\frac{1}{2}y^2}, \tag{9b}$$

where $\hat{U}=\hat{V}$, is an arbitrary constant. After $V$and $U$are solved, the following equation can be obtained according to Eq. (4a):

$$\Phi=\hat{\Phi}\left[\frac{\omega\,(k+\omega)+1}{k}\,y\mathrm{H}_n(y)-\frac{\omega}{\omega^2-k^2}\,\mathrm{H}_{n+1}(y)\right]\mathrm{e}^{-\frac{1}{2}y^2}, \tag{9c}$$

where $\hat{\Phi}=\hat{U}=\hat{V}$, is an arbitrary constant.

It can be seen that factor $\mathrm{e}^{-\frac{1}{2}y^2}$ exists in the expression of both Eq. (6) and Eq. (10). This shows that it decays faster than exponential decay with increasing distance from the equator, which means the disturbance or anomalies may be trapped near the equator. The following is a brief discussion of the dispersion Eq. (8), which is a cubic equation for frequency ω. Three real ω can be obtained with a given wavenumber k (or wavelength) and an integer $n\geqslant 1$. They correspond to a couple of inertial gravitational waves and westward Rossby waves, respectively. The former two are fast waves and the latter is a slow wave. The frequencies of the former two and the latter are absolutely distinguishable. When $n=0$, one solution of Eq. (8) is $\omega=-k$, which corresponds to Rossby-inertial gravitational waves. Besides, there are two inertial gravitational waves propagating eastward and westward, respectively. $n$must be a nonnegative integer in Eq. (8). However, if $n=-1$, the solution of Eq. (8) is $\omega=k$, which is Eq. (5) above, namely, the dispersion relation of Kelvin wave. Thus, the dispersion relation of Kelvin wave is also included in Eq. (8).

$U,\ V$ and Φ in Eqs (6) and (9) are substituted into Eq. (3) and the real part is taken to obtain the solution of the disturbances of waves propagating along the direction of x in the unbounded ocean, i.e., the solution of anomalies. In practice, however, the Pacific, Indian and Atlantic Oceans are invariably bounded at the equator by eastern and western coasts, while none of the above wave solutions satisfy the boundary conditions. Suppose the ocean is bounded by the eastern and western coasts in the north-south direction and its length is $L=L_x$, then the boundary conditions can be represented as

$$x=0,\quad u=0;\qquad x=1,\quad u=0. \tag{10}$$

Then the wave solution satisfying the boundary Eq. (10) can be obtained. As the purpose of this paper is to discuss the interannual and decadal variabilities of abnormal fluctuations, the gravity inertia wave which propagates faster than the Kelvin wave is ruled out. Thus, the Kelvin wave is the only wave propagating eastward. It can be seen from Eq. (6a) that U reaches the maximum at the equator. After ruling out the gravity inertia wave propagating westward, the mixed Rossby inertial-gravity wave and the Rossby wave are the only westward travelling waves. For the former, as can be seen from Eq. (9b), $\mathrm{H}_1(y)=2y$ when $n=0$, and $U$is 0 at the equator where $y=0$, obviously making it impossible be superposed on Kelvin waves to satisfy the boundary Eq. (10). Therefore, Kelvin waves superposed on Rossby waves must be considered to see if it satisfies the boundary Eq. (10). To explore the interannual and decadal variabilities of the abnormal fluctuations as mentioned above, the lowest frequency modes should be considered first. Now examine the structure of Rossby waves with the lowest frequency in the direction of y. Here, we might take $n=1$. In addition, as fluctuations are trapped near the equator, it is only necessary to study the situations near the equator. If $n=1$, noticeably $\mathrm{H}_1=2y$ and $\mathrm{H}_2=4y^2-2$, it can thus be derived that:

$$\begin{aligned}U&=\hat{U}\left[-\frac{k\mathrm{H}_2(y)}{\omega^2-k^2}+(k+\omega)\,y\mathrm{H}_1(y)\right]\mathrm{e}^{-\frac{1}{2}y^2}\\&\approx\hat{U}\frac{2k}{\omega^2-k^2}\,\mathrm{e}^{-\frac{1}{2}y^2}.\end{aligned} \tag{11a}$$

The structure of Eq. (11a) is the same with that of Eq. (6a) in the direction of y. When $y\approx 0$, it can be written as

$$V=\hat{V}\cdot \mathrm{H}_1(y)\cdot \mathrm{e}^{-\frac{1}{2}y^2}\approx 0, \tag{11b}$$

$$\begin{aligned}\Phi&=\hat{\Phi}\left[\frac{\omega\,(k+\omega)+1}{k}\,y\mathrm{H}_1(y)-\frac{\omega}{\omega^2-k^2}\,\mathrm{H}_2(y)\right]\mathrm{e}^{-\frac{1}{2}y^2}\\&\approx\hat{\Phi}\,\frac{2\omega}{\omega^2-k^2}\,\mathrm{e}^{-\frac{1}{2}y^2}.\end{aligned} \tag{11c}$$

As Eq. (11b) shows, $V\approx 0$. It can also be found that the structure of Φ is the same with Eq. (6b) in the direction of y. Thus we can consider the superposition of eastward travelling Kelvin waves and westward travelling Rossby waves when $n=1$. Here, take the frequency ω_0 of Kelvin wave, wave number k_1 and integral constant $\tilde{U}$. Then the solution of eastward travelling waves in an unbounded ocean is (substitute Eq. (6a) into Eq. (3) and take the real part of it)

$$u_1=\tilde{U}_1\mathrm{e}^{-\frac{y^2}{2}}\cos\left(k_1x-\omega_0t\right). \tag{12a}$$

Take the frequency $-\omega_0$ of Rossby wave, when $n=1$, wave

numbers k_2 and integral constant $\hat{U}$. Then the solution of westward travelling waves in an unbounded ocean is (substitute Eq. (11a) into Eq. (3) and take the real part of it)

$$u_2 = \hat{U}_2 \frac{2k_2}{\omega_0^2 - k_2^2} \mathrm{e}^{-\frac{1}{2}y^2} \cos(k_2 x + \omega_0 t). \tag{12b}$$

Equations (12a) and (12b) are both solutions of Eq. (2). The equations are homogeneous linearity equations and satisfy a superposition principle. Therefore, the solution $u_0 = u_1 - u_2$ after superposing two waves is also the solution of Eq. (2). Now, take integral constants $\tilde{U}_1 = U_0$ and $\hat{U}_2 = U_0\left(\omega_0^2 - k_2^2\right)/(2k_2)$. Then

$$\begin{aligned} u_0 = u_1 - u_2 &= U_0 \mathrm{e}^{-\frac{y^2}{2}} \left[\cos(k_1 x - \omega_0 t) - \cos(k_2 x + \omega_0 t)\right] \\ &= -2U_0 \mathrm{e}^{-\frac{y^2}{2}} \sin\left(\frac{k_1 + k_2}{2} x\right) \sin\left(\frac{k_1 - k_2}{2} x - \omega_0 t\right). \end{aligned} \tag{13}$$

Equation (5) shows that $k_1 = \omega_0 \cdot \varepsilon \left[(-\omega_0)^2 - k_2^2\right] - k_2/(-\omega_0) = 3$ can be gotten from Eq. (8). For convenience's sake while not sacrificing generality, we take a long wave approximation, i.e., take $\varepsilon = 0$. Here, the dispersion relation of Rossby wave is $k_2 = 3\omega_0$ and $k_2 = 3k_1$ can be derived. Substituting this into Eq. (13), we can get

$$u_0 = U_0 \mathrm{e}^{-\frac{y^2}{2}} \cdot \sin(2k_1 x) \cdot \sin(k_1 x + \omega_0 t). \tag{14a}$$

In the above equation, the integral constant is still denoted by U_0. The equation is a wave packet and satisfies Eq. (2). Here, we have

$$v_0 = v_1 - v_2 = 0, \tag{14b}$$

$$\eta_0 = \eta_1 - \eta_2 = \Phi_0 \mathrm{e}^{-\frac{y^2}{2}} \sin(2k_1 x) \sin(k_1 x + \omega_0 t), \tag{14c}$$

Equation (14a) can now be examined to see whether it satisfies the boundary Eq. (10). Obviously, it satisfies the conditions that $x = 0, \quad u_0 = 0$. In addition, when $x = 1$, if it satisfies the relation $k_1 = l\pi/2$, here l being an integer and a mode number, then it also satisfies the boundary condition $x = 1,\ u_0 = 0$. We can therefore see that wave number k_1 of Kelvin wave cannot be arbitrary, and can only take discrete values satisfying the relationship $k_1 = l\pi/2$ (for l is a positive integer). Once mode number l is determined, then wave number k_1 is fixed, and according to Eq. (5), the frequency is also determined. Therefore, the absolute value of the frequency of the corresponding Rossby wave equals the frequency of the Kelvin wave and the wave number of the Rossby wave is three times of that of the Kelvin wave.

Finally, in order to discuss and compare with actual ocean situations, the above dimensionless solution is converted to a dimensional one. The following dimensional quantity is

$$x = 0, \quad u = 0; x = L, \quad u = 0, \tag{15}$$

where L is the length of the bounded ocean. The wave number of the Kelvin wave can only be $k_1 = l\pi/L$. Thus the solution satisfying Eq. (1) and boundary Eq. (15) at the same time near the equator is

$$\begin{aligned} u_0 = {} & U_0 \mathrm{e}^{-\frac{\beta}{2c_0}y^2} \sin\left(\frac{l\pi}{L} x\right) \sin\left(\frac{l\pi}{2L}(x + c_0 t)\right) \\ & l = 1,\ 2,\ 3,\ \cdots, \end{aligned} \tag{16a}$$

$$v_0 = 0, \tag{16b}$$

$$\eta_0 = \frac{c_0}{\hat{g}} u_0. \tag{16c}$$

Note that all variables and parameters in the above Eq. (15) are dimensionless. It can be seen from Eq. (16) that the solution is a wave package and its envelope is a sine wave unchanged with time, of which the wave number is $l\pi/L$ and the wave length is $2L/l$. The carrier frequency is a sine wave propagating westward and its wave number is $l\pi/(2L)$, the wave length is $4L/l$, the wave speed is $c_0 = \sqrt{\hat{g}\bar{H}}$, the oscillation frequency is $\sigma = l\pi c_0/(2L) = l\pi\sqrt{\hat{g}\bar{H}}/(2L)$ and the oscillation period is $T = 4L/(lc_0) = 4L/\left(l\sqrt{\hat{g}\bar{H}}\right)$. The frequency σ and the period T is also the respective frequency and period of the bounded equatorial ocean wave packet.

3 Analysis and discussion

In the following calculations, take the standard depth of the upper ocean $\bar{H} = 200$ m, take $(\rho_2 - \rho_1)/\rho_2$ coefficient 1.704×10^{-5} and acceleration of gravity $g = 9.8$ m/s^2. In this case $\hat{g} = 1.67 \times 10^{-4}$ and $c_0 = \sqrt{\hat{g}\bar{H}} = 0.183$ m/s. Then take $\beta = 2.289 \times 10^{-11}$ m$^{-1}\cdot$s^{-1} and $U_0 = 0.02$ m/s. Thus $\beta/(2c_0) = 6.26 \times 10^{-11}$. Note that these environmental parameters are not related to the length of the bounded ocean L or mode number l.

3.1 *Results regarding the equatorial Pacific*

The following are calculation results regarding the equatorial Pacific. The equatorial Pacific Ocean spans a distance of approximately 160° at longitude in the east-west direction. Take the distance L=17 600 km.

(1) The result of Mode 1.

Take mode number $l = 1$, and the images of the abnormal wave packet of the equatorial Pacific Ocean can be obtained from Eq. (16). Figure 1 shows the wave form of zonal flow anomalies of the ocean wave packet, i.e., the wave form of u, when $y = 0$ at time $t = 0,\ T/8,\ T/4,\ 3T/8,\ T/2,\ 5T/8,\ 3T/4,\ 7T/8,\ T$. Here, take L=17 600 km, and the corresponding oscillation frequency of the wave packet is $\sigma = 1.631 \times 10^{-8}$ s^{-1}, the oscillation period $T = 12.21$ a, manifesting decadal variability. The figure shows that the zonal flow anomaly is 0 in the east-west coast of the equatorial ocean, which satisfies the boundary Eq. (15). The zonal flow anomalies show consistency across the entire ocean most of the time, i.e., half-wave abnormality. It shows an abnormal wave in a rather short period only when conversion occurs in the zonal flows (at the moment $3T/8$ and $7T/8$) with a rather small abnormality value. The wave form is restored to that in the starting time at the end of a cycle. The amplitude of the zonal flow anomaly of the ocean wave packet is about 0.02 m/s. As $\eta_0 = (c_0/\hat{g})\, u_0$, the wave form of upper depth (thickness) anomaly of the ocean wave packet at the equator ($y = 0$) at the above moments is the same as in Fig. 1. The thickness anomalies, with an approximate amplitude of 22 m, also show consistency across the entire ocean most of the time.

Figure 2 is the vector diagram of flow field anomalies of the

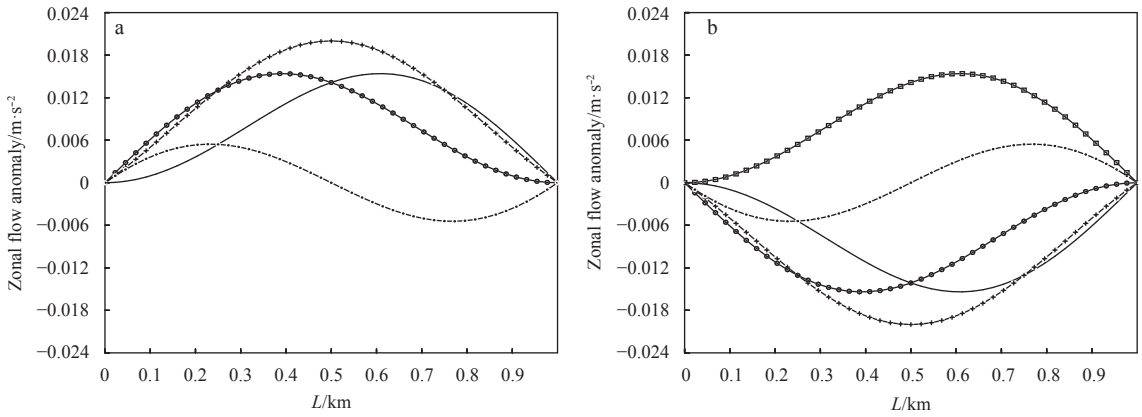

Fig. 1. The wave form of zonal flow anomalies of the ocean wave packet at the equator at different time of Mode 1. The solid line, the cross line, the hollow round line and the solid round line represent the wave form in time 0, $T/8$, $T/4$ and $3T/8$, respectively. In Fig. 1a, T represents period and T=12.21 a; and in Fig. 1b, the solid line, the cross line, the hollow round line, solid round line and the hollow block line represent the wave form in time $T/2$, $5T/8$, $3T/4$, $7T/8$ and T.

wave packet in a range of 1 000 km (about 10°) to the equator in this mode when t=0, $T/4$, $T/2$, $3T/4$. The figure shows that the meridional flow anomaly is 0 and the zonal flow anomalies are invariably in the east-west direction at the above moments. The flow field anomalies reach the maximum in the central equatorial ocean and decay rapidly away from the equator, and are limited to within a range of about 2° of the equator. Besides, the flow field anomalies show very strong characteristics of equatorially trapped waves. On the east and west coasts of the ocean, the flow field anomaly is always 0, which satisfies the above boundary conditions. When t=$3T/8$ or t=$7T/8$, the time when the flow field anomaly changes its direction, the consistent east-west flow is disrupted (figure omitted).

Figure 3 shows the distribution of thickness anomalies of the wave packet in the same range of Fig. 2 when $t=0$, $T/4$, $T/2$, $3T/4$, respectively. As can be seen from this figure, the thickness anomalies show consistency across the entire ocean at the above moments, indicating half-wave abnormality. The anomaly is 0 on the east and west coasts. Its absolute value reaches the maximum at the center of the ocean and decays rapidly away from the equator, and is limited to within a range of about 2° of the equator, which is the same as that of the above mentioned flow anomalies. When $t = 3T/8$ or $t = 7T/8$, which is the time of positive-negative conversion of the thickness anomalies, the consistency of the thickness anomalies is disrupted (figure omitted).

(2) The result of Mode 2

Take mode number $l = 2$ and the images of anomalies of the wave packet of the equatorial Pacific Ocean can be obtained from Eq. (16). Figure 4 shows the wave form of the zonal flow anomalies of the ocean wave packet, namely, the wave form of u, when $y = 0$ at time$t = 0$, $T/8$, $T/4$, $3T/8$, $T/2$, $5T/8$, $3T/4$, $7T/8$, T. Here, take L=17 600 km, and the corresponding oscillation frequency of wave packet is 3.262×10^{-8} s^{-1}, the oscillation period is T=6.10 a, manifesting interannual variability. As can be seen from the figure, the zonal flow anomaly is always 0 on the east-west coasts of the equatorial ocean, which satisfies the boundary Eq. (15). In stark contrast to Mode 1 (Fig. 1), at this time there is a stagnation point at the center of the ocean, where the zonal flow anomaly is always 0. This stagnation point splits the ocean into eastern and western halves. The amplitude of zonal flow anomalies of the ocean wave packet is also about 0.02 m/s. The wave form of the upper depth (thickness) anomaly of the ocean wave packet at the equator ($y = 0$) at the above moments is the same as in Fig. 4, also with an approximate amplitude of 22 m.

Figure 5 is the vector diagram of flow field anomalies of the wave packet in the range of 1 000 km (about 10°) to the equator in this mode when $t = 0$, $T/4$, $T/2$, $3T/4$. In this figure, the meridional flow anomaly is also 0, and the zonal flow anomalies decay rapidly away from the equator with the same speed as that of Mode 1 and are limited to within a range of about 2° of the equator. Besides, the flow field anomalies show very strong characteristics of equatorially trapped waves. The flow field anomalies are always 0 on the east and west coasts of the ocean, which satisfies the above boundary conditions, as well as at the center of the ocean. As shown in Figs 4 and 5, the direction of zonal flow anomalies of Mode 2 is consistent in the eastern half of the ocean most of the time, and so is in the western half. However, the directions of the flow in the eastern and western half might be the same or opposite. In this case, the zonal flow anomalies of this mode are semi-wave abnormalities in the eastern half of the ocean. When $t = 3T/8$ and $t = 7T/8$, the time when the flow field anomaly changes direction, there will be a one-wave anomaly lasting for a rather short period in half of the ocean within this range, with a rather small value. Situations are the same in the western half of the ocean except that the time is $3T/8$ and $5T/8$. Notice that the above half-wave and one-wave analysis is for half of the ocean. More complex analysis is needed for the entire ocean when the eastern and western halves of the ocean are both taken into consideration.

Figure 6 shows the distribution of thickness anomalies of Mode 2 when $t = 0$, $T/8$, $T/4$, $3T/8$, $T/2$, $5T/8$, $3T/4$, $7T/8$, respectively. More diagrams are given regarding mode 2 than Mode 1 for the sake of the following discussion. As can be seen from this figure, the thickness anomalies of the wave packet is consistent with the same sign in the eastern and the western half of the ocean. Its absolute value reaches the maximum at the center of the ocean and decays rapidly to the north and south sides of the equator at the same speed as that of Mode 1. This thickness anomaly is also limited to within a range of about 2° of the equator and trapped near the equator. The anomaly is always 0 at the east and west coasts as well as at the center of the ocean, which is different from Mode 1 (Fig. 3).

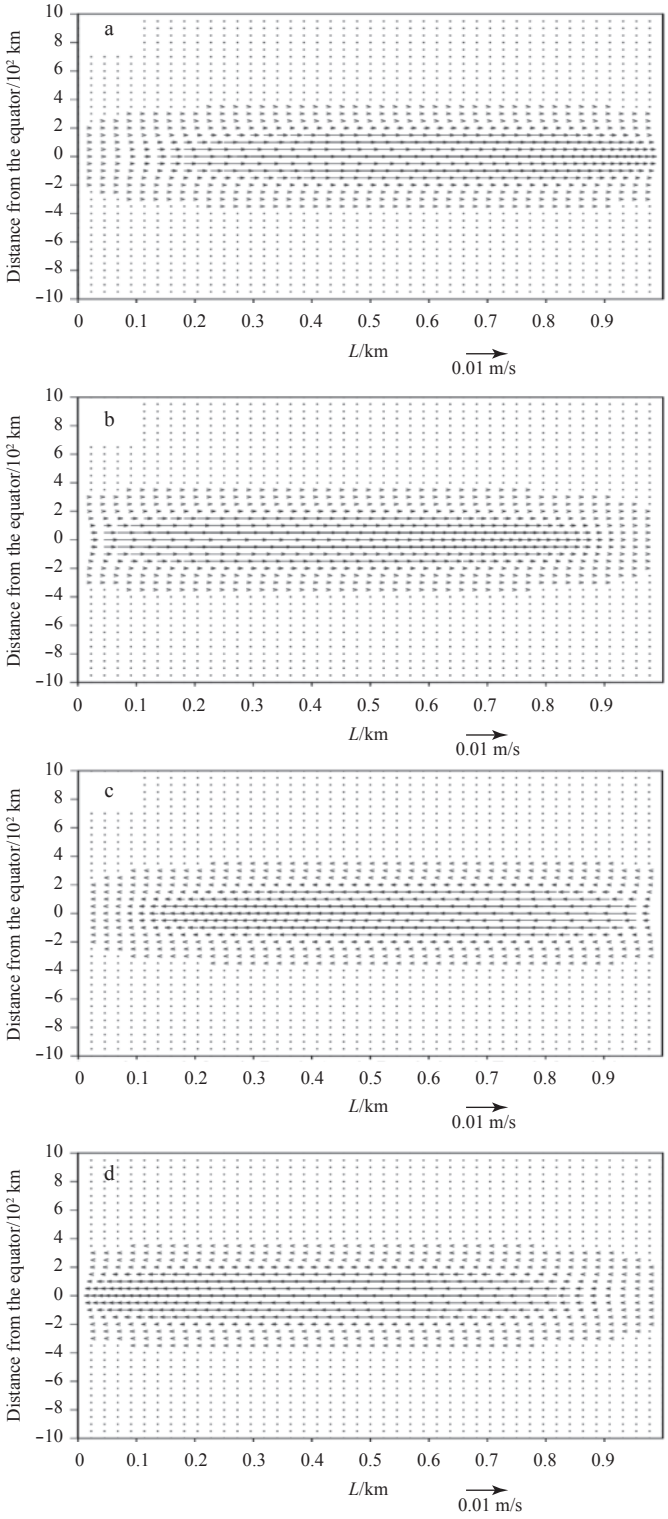

Fig. 2. Vector diagram of flow field anomalies of Mode 1. a. t=0, b. t=T/4, c. t=T/2, and d. t=3T/4.

3.2 *The results of the equatorial Indian Ocean and the Atlantic Ocean*

As all environment parameters in this paper are the same as the above beside the length of the ocean in the east-west direction, the wave form of the ocean wave packet and its attenuation to the north and south of the equator are the same, except that difference in length L of the equatorial Indian Ocean and the equatorial Atlantic Ocean in the east-west direction will affect the oscillation frequency and period of the wave packet of each mode. This section gives the results in this regard. While the above figures show the wave form, we will only replace L in these figures with the length of the equatorial Indian Ocean and the equatorial Atlantic and T with the oscillation period of the equatorial Atlantic and the equatorial Indian Ocean.

(1) The results regarding the equatorial Indian Ocean

First, as to Mode 1 results of the equatorial Indian Ocean, take

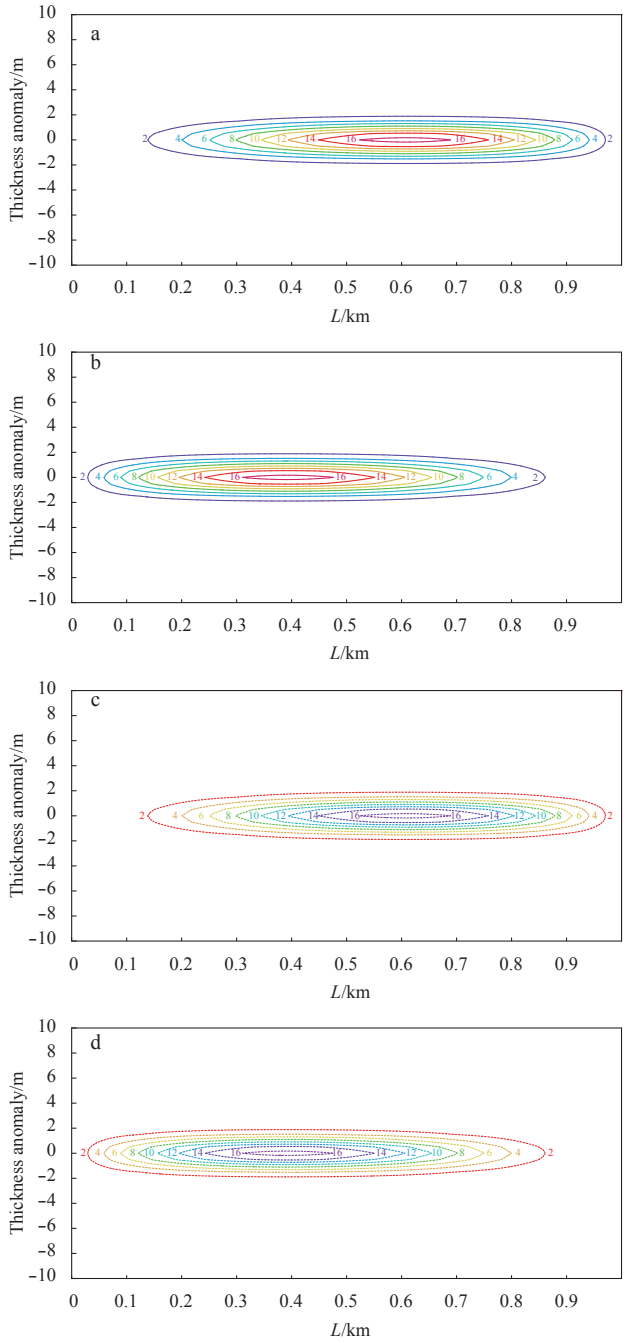

Fig. 3. The distribution of thickness anomalies of Mode 1. a. t=0, b. t= T/4, c. t= T/2, and d. t=3T/4.

mode number $l = 1$, and L=7 700 km as the equatorial Indian Ocean in the east-west direction spans about 70° degrees at longitude. The results indicate that the oscillation frequency is $\sigma = 3.729 \times 10^{-8}$ s^{-1} and the period is $T = 5.34$ a for Mode 1, manifesting the interannual variability. Then, as to Mode 2 results of the equatorial Indian Ocean, take mode number $l = 2$ and L= 7 700 km. The results indicate that the oscillation frequency is $\sigma = 7.457 \times 10^{-8}$ s^{-1} and the period is $T = 2.67$ a for Mode 2, also manifesting the interannual variability. The above results illustrate that the oscillation frequency of the wave packet is higher than that of the equatorial Pacific Ocean while the period is shorter than that of the equatorial Pacific Ocean because the length of the equatorial Indian Ocean in the east-west direction is smaller than that of the equatorial Pacific Ocean.

(2) The results regarding the equatorial Atlantic

First, as to Mode 1 results of the equatorial Atlantic Ocean, take mode number $l = 1$ and L=4 950 km as the equatorial Atlantic Ocean in the east-west direction spans about 45° at longitude. The results indicate that the oscillation frequency is $\sigma = 5.800 \times 10^{-8}$ s^{-1} and the period is $T = 3.43$ a for Mode 1, manifesting the interannual variability. Then, as to Mode 2 results of the equatorial Atlantic Ocean, take mode number $l = 2$ and L= 4 950 km. The results indicate that the oscillation frequency is $\sigma = 1.160 \times 10^{-7}$ s^{-1} and the period is $T = 1.72$ a for Mode 2, also manifesting the interannual variability. The above results illustrate that the oscillation frequency of the wave packet is high-

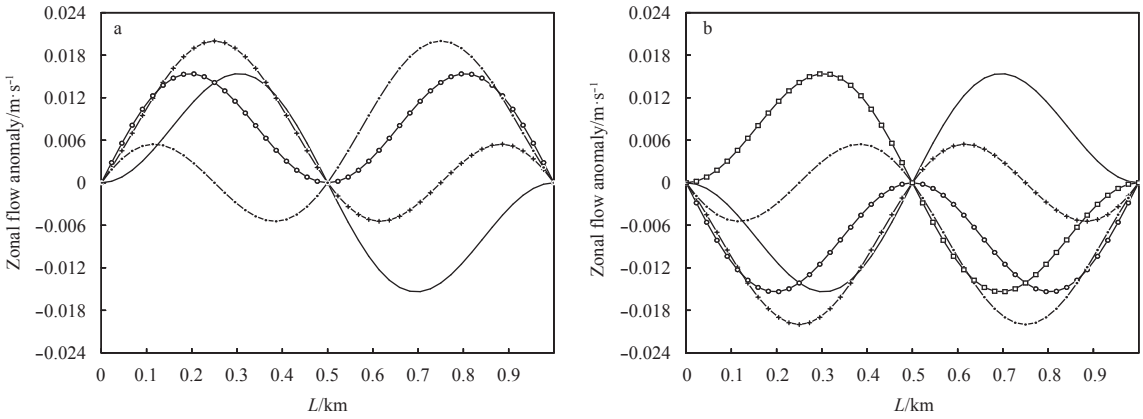

Fig. 4. The wave form of zonal flow anomalies of the ocean wave packet at the equator at different time of Mode 2. The solid line, the cross line, the hollow round line and the solid round line represent the wave form in time 0, $T/8$, $T/4$ and $3T/8$, respectively. In Fig. 4a, T represents period and T=6.10 a; and in Fig. 4b, the solid line, the cross line, the hollow round line, solid round line and the hollow block line represent the wave form in time $T/2$, $5T/8$, $3T/4$, $7T/8$ and T .

er than that of the equatorial Pacific Ocean and the period is shorter than that of the equatorial Pacific Ocean because the length of the equatorial Atlantic Ocean in the east-west direction is smaller than that of the equatorial Pacific Ocean.

3.3 *Discussion of solution of the wave packet*

First, as to the speed of decay of wave packet anomalies in a bounded equatorial ocean away from the equator, it depends on the value of $\beta/(2c_0)$. Because β of the earth is a constant, so the value is inversely proportional to $c_0 = \sqrt{(\rho_2 - \rho_1)/\rho_2 g\bar{H}} = \sqrt{\hat{g}\bar{H}}$. The smaller c_0 is, the faster the wave packet decays away from the equator. In fact, given the difference of $(\rho_2 - \rho_1)/\rho_2$ and $\bar{H}$ in the above three oceans, the value of c_0 will vary slightly, but should be similar in general, thus $c_0$in this paper is given the same value, resulting in the same value of $\beta/(2c_0)$. This suggests identical degree of attenuation of the wave packet anomalies to the north and south sides of the equator.

Then, as to the relationship between the wave packet anomalies and the mode number l, when $l = 1$, the wave packet anomalies across the entire ocean appear in semi-wave forms most of the time (Figs 1–3). The wavelength of the wave packet anomalies is twice that of the entire ocean in the east-west direction on the equator. When $l = 2$, the wave packet anomaly appears in the semi-wave form (Figs 4–6) in half of the ocean most of the time. The greater the mode number l, that is, the higher the wave mode, the shorter the wavelength of the wave packet anomaly.

Moreover, regarding the oscillation frequency and period of the wave packet anomalies, the solution of the equatorial wave packet in a bounded ocean as studied in this paper is a free fluctuation satisfying the lateral boundary conditions in a bounded ocean. When length L of a bounded equatorial ocean in the east-west direction, mode number l and the phase velocity of equatorial Kelvin wave are determined, the oscillation frequency and period can also be determined. As the value of c_0 is constant in this paper, the oscillation frequency (period) depends only on the scale of the bounded ocean on the equator and the mode number, and therefore the oscillation frequency of the wave packet is the natural frequency of the ocean. It can be seen from Eq. (16) that the longer length L of the equatorial ocean in the east-west direction and the smaller mode number l, the lower the natural frequency of the wave packet anomalies and the longer the period and wavelengths. The oscillation of the wave packet manifests the interannual and decadal variabilities for low modes (Mode 1 or 2) regarding the length in the east-west direction of the three oceans on the equator.

Finally, regarding the flow field anomalies of the equatorial ocean wave packet and depth (thickness) anomalies, the corresponding thickness anomalies are positive (negative) in the range of east (west) ward propagating flow anomalies close to the equator. The absolute value of the thickness anomalies reaches a maximum when the absolute value of the flow field anomalies is at the maximum, which can be understood from analyzing Eqs (16a) and (16c) (Figs 2, 3, 5 and 6). Thus, the configuration of flow field and depth (thickness) anomalies is consistent with the classic equatorial Kelvin wave (Zhang and Zhang, 2006). It is worth noting that the thickness anomalies of the upper ocean can reflect the temperature anomalies of the upper ocean to a certain extent despite the fact that the temperature cannot be introduced in the above shallow water (positive) mode. The temperature anomaly of the upper ocean is positive (negative) when the thickness anomaly is positive (negative), which will be needed in the following examination of the relationship of the wave packet with the ENSO and the IOD (Indian Ocean dipole).

4 Comparison with actual equatorial oceans

4.1 *Comparison with the actual equatorial Pacific*

We have conducted the complex EOF analysis of the flow field anomalies on the ocean surface (hereinafter referred to as the former) in multiple years in the tropical Pacific in winter, spring, summer, and autumn (represented by January, April, July and October, respectively) (Lu et al., 2014), and found that the distribution of the flow field anomalies corresponding to the wave packet anomalies calculated from Section 3.1 when $l = 1$ (hereinafter referred to as the latter) in the equatorial Pacific Ocean is very similar to the spatial distribution of the first mode of the former. The first mode of the former is a zonal flow with the same direction near the equator throughout the Pacific with almost no meridional flow. Its flow field is also trapped near the equator [see Fig. 1 in Lu et al., (2014)]. When $l = 1$, the oscillation period

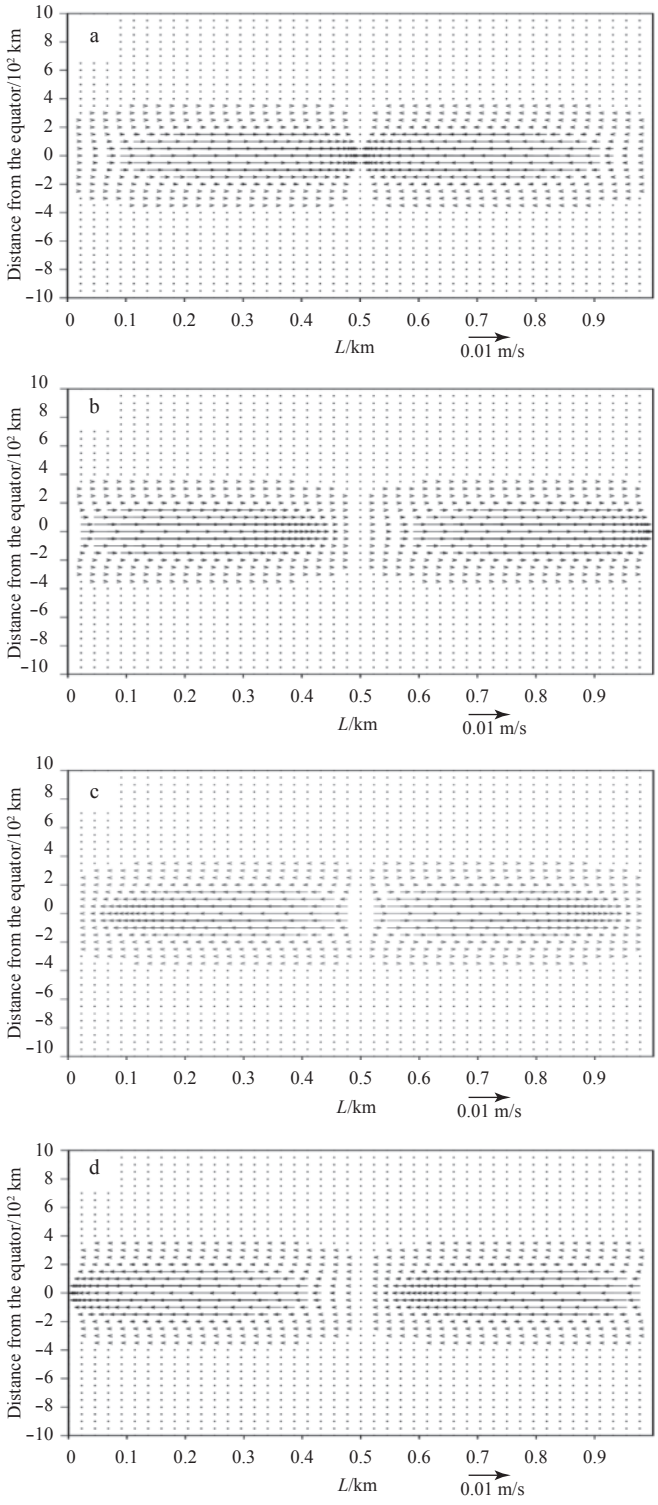

Fig. 5. The vector diagram of flow field anomalies of Mode 2. a. t=0, b. t= T/4, c. t= T/2, and d. t=3T/4.

of the latter is 12.21 a as discussed above, which manifests the decadal variability. Lu et al. (2014) conducted the wavelet analysis of the real time coefficient of the first mode of the former, and found significant decadal variability of 14 a and 16 a (Figs 4a and c in Lu et al., (2014)). The decadal variability period of the former in that mode in winter and summer is similar with the oscillation period of Mode 1 of the latter, especially in winter. Thus the first mode of the complex EOF analysis for the equatorial Pacific in winter and summer is equivalent in nature to the wave packet anomalies in the equatorial Pacific Ocean of Mode 1. Therefore the wave packet anomalies of Mode 1 in this paper exist in actual situations. It has also been proposed that the nature of the first mode of the former is equatorial Kelvin wave anomalies (Lu et al., 2014). Seen from the present, this judgment is still not accurate because the anomalies of pure equatorial Kelvin waves do not satisfy the boundary conditions of east and west coasts. However,

as Lu et al. (2014) suggested, the equatorial Kelvin wave anomalies indeed play an important role here as one of the two components of the wave packet solutions.

It has also been found that the flow field distribution of Mode 2 of the latter is also similar to the distribution of the second mode of anomalies in surface flow field of the former. Both of them appear as waves trapped near the equator and a disruption is observed in consistent zonal flow anomalies across the ocean, with the zonal flow anomalies in opposite directions in the eastern and western ocean (Fig. 5 herein and Fig. 5 in reference Lu et al., (2014)). The wavelet analysis of time coefficient of the second mode of the former indicates a very significant variation period of

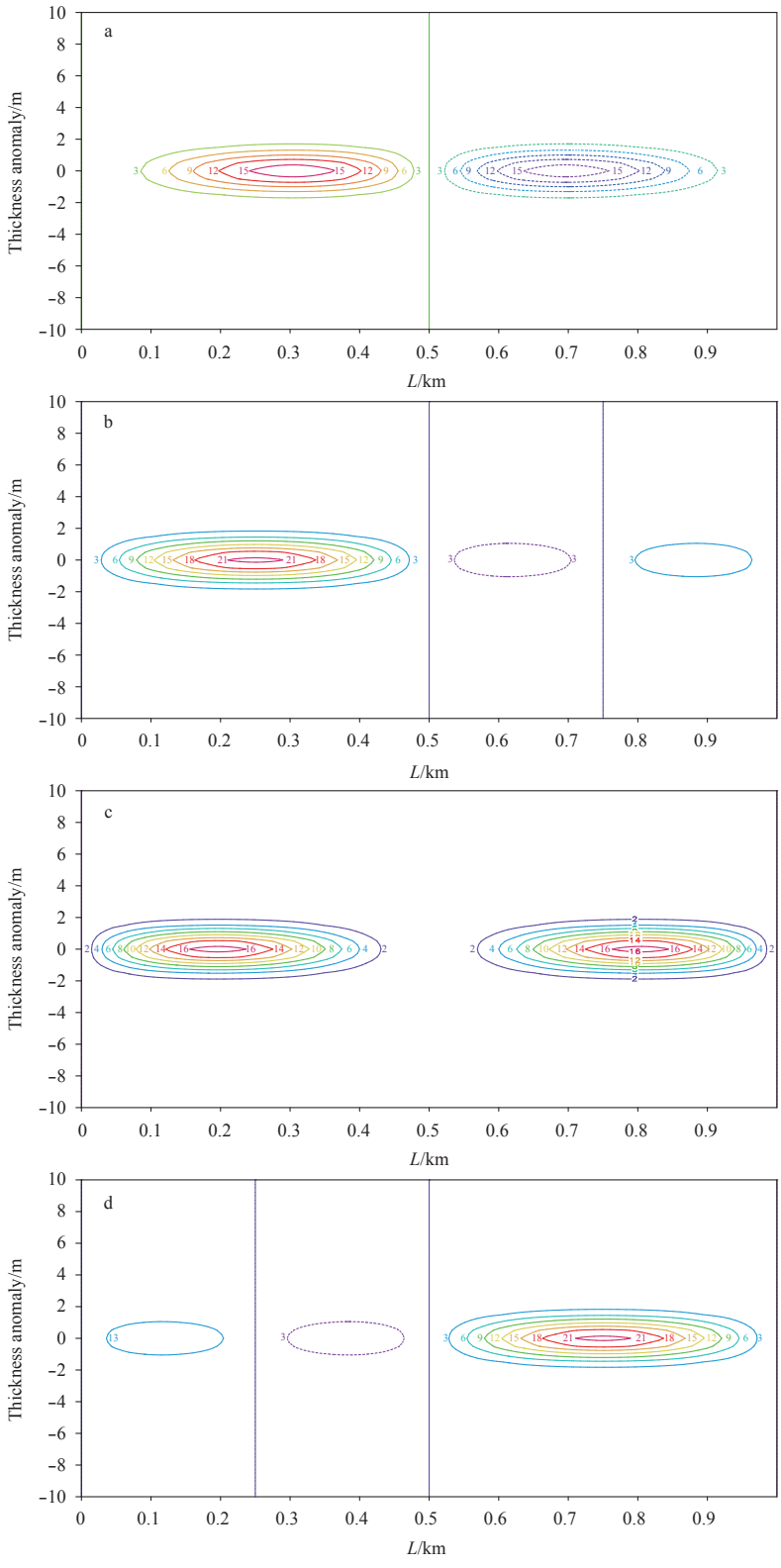

Fig. 6.

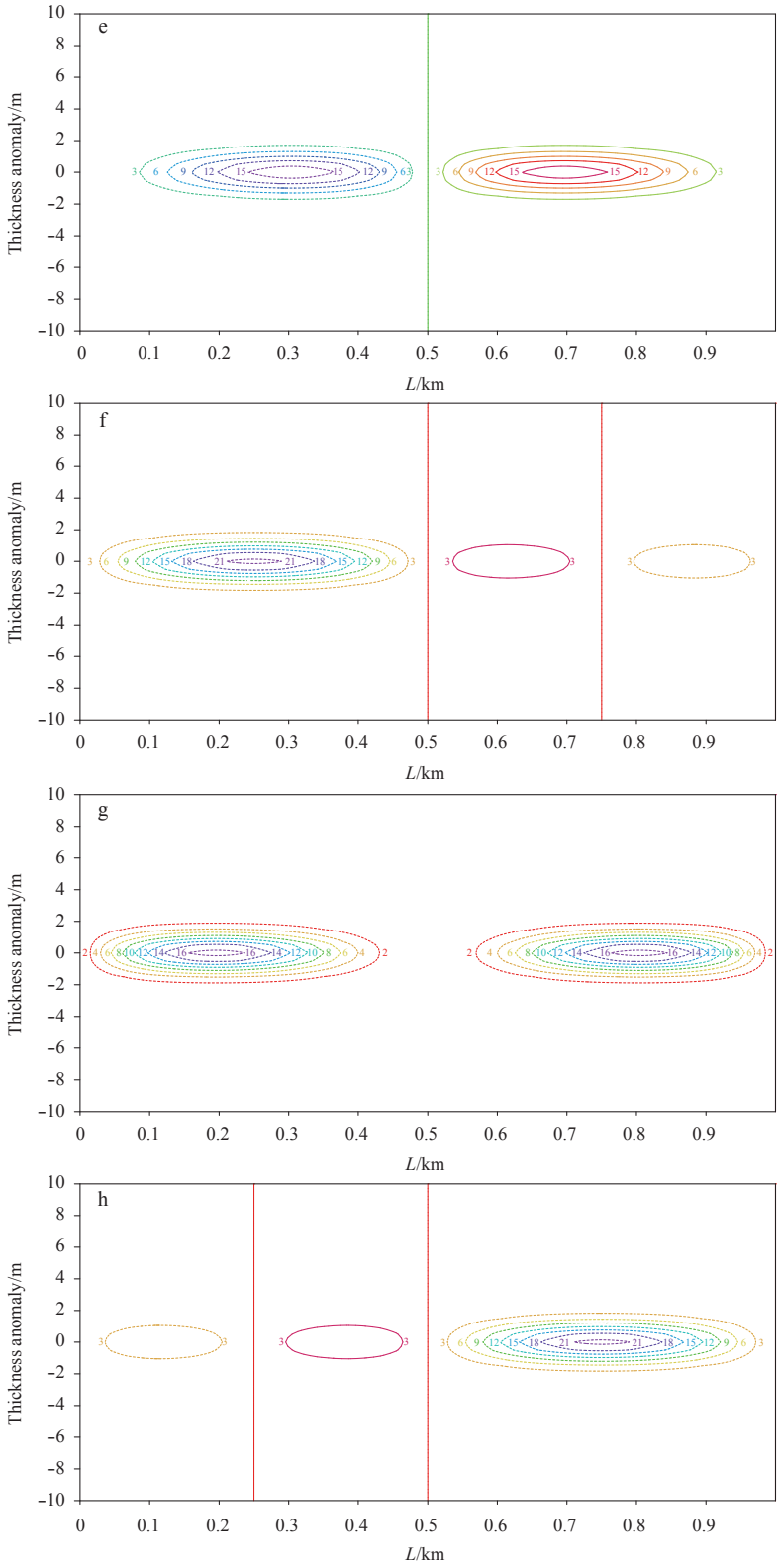

Fig. 6. Distribution of thickness anomalies of Mode 2. a. t=0, b. t= T/8, c. t= T/4, d. t=3T/8, e. t= T/2, f. t=5T/8, g. t.=3T/4, and h. t=7T/8.

6 and 7 a in winter and summer, respectively (Lu et al. 2014). The oscillation period of Mode 2 of the latter is 6.1 a as discussed above. The period of interannual variability of the second mode of the former and the oscillation period of Mode 2 of the latter are both manifested as the interannual variability in winter and summer, being very close to each other in value, and almost identical in winter. From the wave form and period of flow field anomalies on the equator, we may consider the second mode of the complex EOF analysis for flow field anomalies in the equatorial Pacific in winter and summer as equivalent in nature to the wave packet anomalies in the equatorial Pacific Ocean of Mode 2.

4.2 *Comparison with the actual equatorial Indian Ocean and Atlantic Ocean*

4.2.1 *Comparison with the actual equatorial Indian Ocean*

We conducted the complex EOF analysis of the flow field anomalies on the surface of the tropical Indian Ocean in May and October (Zhang, 2006; Zhang and He, 2005), and found that the flow field distribution of the wave packet anomalies (the latter) in the equatorial ocean of Mode 1 obtained by taking the length of the equatorial Indian Ocean in the east-west direction in Section 3.2 is also very close to the surface distribution of the first mode of the former (Fig. 6.1–1 in Zhang (2006) and Fig. 2 in Zhang and He (2005)). The spatial field of the first mode of the former appears as consistent zonal flows throughout the Indian Ocean trapped near the equator. The oscillation period of Mode 1 of the latter is 5.34 a as described above and the changing period of the modulus of the complex time coefficient of the first mode of the former is 4 a (Figs 6.1–7 in Zhang (2006)). Thus the period of interannual variability of the first mode of the former is very close to the oscillation period of Mode 1 of the latter. The above analysis indicates that the first mode is equivalent in nature to the wave packet anomalies of Mode 1 in the equatorial ocean.

The surface spatial distribution of the second mode of the former is also similar to the distribution of the flow field of Mode 2 of the latter. The consistent zonal flow anomalies throughout the ocean are now disrupted and may have opposite directions in the eastern and western parts of the ocean (Figs 6.1–3 in Zhang (2006)) and Fig. 6 in Zhang and He (2005)). The oscillation period of Mode 2 of the latter is 2.67 a as discussed above while the changing period of the modulus of the complex time coefficient of the second mode of the former is 4 a (Figs 6.1–8 in Zhang (2006)). The values of the former and the latter are close, again indicating that the second mode is in nature the wave packet anomalies of Mode 2 in the equatorial Indian Ocean.

Xuan et al. (2014) showed the distribution of surface currents of the tropical eastern Indian Ocean through OSCAR in May and found rapid eastward jets in the equatorial waters in a range of (2°S–2°N) with a maximum speed of 0.7 m/s, and identified them as Wyrtki jets (Fig. 3 in Zhang and He (2005)) The position and distribution of the jets show great similarity to the first mode of the wave packet solution. Thus the jets can been seen as the wave packet solution in the equatorial Indian Ocean.

Dong et al. (2016) provided the results of the complex EOF analysis based on SST data in the Indian Ocean, where the spatial field of the first mode shows a positive SST anomaly distribution across the entire equatorial Indian Ocean, with the strongest positive anomaly observed at the center of the ocean (Fig. 2 in Dong et al. (2016)), which is very similar to the thickness anomaly distribution of Mode 1 of the wave packet discussed in this paper (Fig. 3).

The above analyses indicate that the solution of the wave packet exist in the actual equatorial Indian Ocean.

4.2.2 *Comparison with the actual equatorial Atlantic Ocean*

As no complex EOF analysis for the flow field anomalies in the tropical Atlantic has been conducted to the best of our knowledge, no detailed discussion of the wave packet anomalies in the equatorial Atlantic is provided here. However, past research has shown by analyzing the principal component of ship data that the maximum of the first principal component of upper-ocean sea surface temperature anomalies (SSTA) in the tropical Atlantic occurs on the equator and shows a quasi-biennial variability (Houghton and Tourre, 1992). This spatial distribution has similarities with the distribution of thickness anomalies of Mode 1 of the wave packet anomalies in the equatorial Atlantic in Section 3.2. This is because thickness anomalies of the upper layer of sea water may reflect the temperature anomalies of the upper ocean. The oscillation period of Mode 1 of the equatorial Atlantic is 3.43a in Section 3.2, which is close to the quasi-biennial variability as mentioned above.

4.3 *Considering the Indonesian throughflow*

The equatorial Atlantic is self-enclosed, a feature not shared by the equatorial Pacific or Indian Ocean. The Indonesian throughflow travels between the equatorial Pacific and Indian Oceans, through which the equatorial Kelvin waves can enter the equatorial Pacific from the equatorial Indian Ocean, and the tropical Rossby waves can enter the tropical Indian Ocean from the tropical Pacific Ocean. When the throughflow is considered, the length of the bounded ocean on the equator in the east-west direction shall be equal to the sum of the length of the equatorial Indian Ocean and the length of the equatorial Pacific Ocean, i.e., L = 7 700 + 17 600 = 25 300 (km). This paper uses L to calculate the oscillation frequency and period of Modes 1 and 2 of the wave packet of the bounded equatorial ocean. Their respective oscillation frequencies are 1.135×10^{-8} and 2.270×10^{-8} s^{-1}, with corresponding oscillation periods of 17.55 and 8.77 a, showing the decadal variability and the inter annual variability, respectively.

The first mode of this wave packet appears as consistent zonal flow field and thickness anomalies in the equatorial Indian and Pacific Oceans most of the time (Section 3), with a calculated oscillation period of 17.55 a. The real time coefficients of the first mode of flow field anomalies in the actual tropical Pacific show the decadal variability of 22 and 21 a in winter and summer, respectively (Fig. 4 in Lu et al. (2014)). However, the modulus of the complex time coefficient of the first mode of the flow field anomalies shows decadal variability of 18 a in the actual tropical Indian Ocean in May (Figs 6.1–7 in Zhang (2006). The above period of decadal variability of the actual ocean is similar to the oscillation period of Mode 1 of the wave packet, especially in the tropical Indian Ocean in May when the two are almost identical. This suggests that Mode 1 of this wave packet does exist in reality, which is the reason why the tropical Pacific Ocean and the tropical Indian Ocean show the decadal variability of the flow field and thickness anomalies.

There is a stagnation point at the midpoint of the length of Mode 2 of this wave packet L=25 300 km, i.e., around 160°E, where the value of the zonal flow and thickness anomalies is always 0. This stagnation point divides the tropical ocean into eastern and western halves. The western half comprises the tropical Indian and Pacific Oceans west of 160°E, and the eastern half comprises the tropical Pacific Ocean east of 160°E, accounting for most of the entire tropical Pacific Ocean. As the consistency of the flow field and thickness anomalies in the eastern and western halves of the ocean is disrupted, the zonal flow and thickness anomalies in the tropical Indian Ocean and tropical Pacific Ocean may become inconsistent, although the change in zonal flow and thickness anomalies is still consistent in the entire tropical Indian Ocean most of the time. The oscillation period of Mode 2 of this wave packet is 8.77 a. The modulus and argument of the complex time coefficient of the first mode in the flow field anomalies in the tropical Indian Ocean have a decadal variability of 8 a in (Figs 6.1–7 in Zhang (2006)), almost identical to the oscillation period of Mode 2 of this wave packet.

Recent findings by Dong et al. (2016) show that warm SST an-

omalies formed in the eastern tropical Pacific are accompanied by basin-wide warm SST anomalies in the Indian Ocean, and vice versa, which is very similar to the thickness anomaly distribution of Mode 2 after considering the Indonesian throughflow in this paper (Figs 6b and f). Mode 2 has a variability of 8 a and a double period of 16 a, which is very close to decadal variability in the above mentioned findings (Fig. 2 in Dong et al. (2016)). Dong et al. (2016) also found that in the ocean-atmosphere coupled model, once SST changes in the eastern tropical Pacific are given as observed data, then the amplitude and periodic changes of SST decadal variability in the Indian Ocean can be simulated in great detail. This suggests that although human activities have dominated the long-term warming of the Indian Ocean, its decadal variability is mostly determined by the internal variability of the climate system. The results of Mode 2 of the wave packet after considering the Indonesian throughflow can provide physical explanations for these findings (see "(3) Important findings" in Section 4.4)

The above analysis shows that this wave packet can explain the decadal variability of the tropical Pacific Ocean and the tropical Indian Ocean after considering the Indonesian throughflow, whose importance cannot be ignored.

4.4 *Relationship with ENSO and IOD*

The ENSO and the IOD are the most striking phenomena in the tropical Pacific and tropical Indian Ocean, respectively. Many studies have been done on the ENSO and the IOD and most consider them as caused by air-sea interaction (Keller et al., 2015; Sun et al., 2014, Su et al., 2015; Sein et al., 2015). Considering their shared feature as the disruption of inconsistency throughout the tropical ocean, we might interpret them as related to Mode 2 of this wave packet. As discussed above, the thickness anomalies in the upper ocean can reflect the temperature anomalies to a certain extent in the shallow (positive) mode in this paper although the temperature cannot be introduced. When the thickness anomalies are positive (negative), the SSTA in the upper ocean is also positive (negative).

(1) Relationship with the tropical Pacific Ocean

The following is an examination of the relationship between the thickness anomalies of Mode 2 of this wave packet and the ENSO cycle when the length of the equatorial Pacific in the east-west direction L=17 600 km. Figure 6 shows positive and negative thickness anomalies in the eastern and western halves of the equatorial ocean at the initial time when t=0, respectively. When t= T/8 (T is the natural period), positive thickness anomalies in the western half of the ocean reach the maximum value while those of the eastern half are close to the normal value; when t= T/4, the positive anomalies in the western half of the ocean decrease while those in the eastern half increase; when t=3T/8, the positive anomalies in the eastern half of the ocean reach the maximum value while those in the western half are close to the normal value, constituting an El Niño event; when t= T/2, the positive anomalies in the eastern half of the ocean decrease while the negative anomalies in the western half of the ocean increase; when t=5T/8, the negative anomalies in the western half of the ocean reach the maximum value while those in the eastern half are close to the normal value; when t=3T/4; the negative anomalies in the western half of the ocean decrease while those in the eastern half increase; when t=7T/8, the negative anomalies in the eastern half of the ocean reach the maximum value while those in the western half are close to normal value, constituting a La Niña event. When t=T, the distribution of thickness anomalies in the ocean is restored to that at the initial time, completing an ENSO cycle. The natural period of the cycle T is 6.1 a, which falls within a period of 3–7 a in an actual ENSO cycle.

It has been mentioned that the second mode of the complex EOF analysis for the flow field anomalies is also the ENSO mode and has an interannual variability of 5–7 a, which is consistent with the above analysis (Lu et al., 2014). A joint complex EOF analysis has been made for an atmospheric wind field and a flow field in May in the tropical Pacific Ocean (Lu and Zhang, 2009), which shows that its second mode is also the ENSO mode and the modulus and argument of the complex time coefficient of this mode both have an interannual variability of about 5 a (Fig. 6 in Lu and Zhang (2009)), which is very close to the natural period of the above wave packet solution, i.e., 6.1 a. The spatial field on the ocean surface of this mode also shares features of the above wave packet solution (Fig. 4 in Lu and Zhang (2009)).

(2) Relationship with the IOD in the tropical Indian Ocean

The surface of the tropical Indian Ocean demonstrates the typical SSTA, which has huge influence on the climate of the Indian Ocean and its surrounding areas. During positive IOD events, the SSTA is positive in the western equatorial Indian Ocean and negative in the eastern equatorial Indian Ocean, and vice versa during negative IOD events (Yan and Zhang, 2004). Figure 6 suggests obvious negative and positive thickness anomalies in the eastern and western halves of the ocean at the initial time when t=0 and the length of the equatorial Indian Ocean in the east-west direction L=7 700 km, constituting a positive IOD event. There are obvious positive and negative thickness anomalies in the eastern and western halves of the ocean when t= T/2, constituting a negative IOD event. The distribution of the thickness anomalies in the ocean is restored to the positive IOD event at the initial time when t=T, thus completing an IDO cycle. Here the period of cycle is 2.67 a.

Although Zhang (2006) and Zhang and He (2005) both mentioned that the second mode of the complex EOF for the flow field anomalies is associated with the ENSO, strong upward and downward flows are present in the eastern and western equatorial Indian Ocean, respectively, from the vertical motion field near the equatorial surface in the two studies. Corresponding to a vertical field, obvious cold and warm anomalies exist in the eastern and western equatorial Indian Ocean in the temperature field near the surface, which is exactly the configuration of the SST anomalies during the positive IOD events. When the argument of complex time coefficient is inverse (Figs 6.1–6 in Zhang (2006) and Fig. 9 in Zhang and He (2005)), the configuration during the negative IOD events is formed. This second mode has a 4a interannual variability, which is also similar to the oscillation period of 2.67 a of Mode 2 of the above wave packet solution.

(3) Important findings

The above discussion about the wave packet solution of the bounded ocean shows that the oscillation frequency of the wave packet is the natural frequency of the ocean. It depends only on the length L of the bounded equatorial ocean in the east-west direction when the phase velocity c_0 of the Kelvin wave is determined. The principle of resonance in physics suggests that the bounded ocean will resonate with the external forces (such as wind stress and air-sea interaction, etc.). Once the changing frequency of the external forces and the natural frequency are identical or similar, resulting in the rapid increase of the amplitude of the natural frequency of disturbances (anomalies) of the wave packet, in other words, strong responses from the bounded ocean to the external forces. If the frequency of the external forces is vastly different from that of the natural frequency of the ocean, the response would not be strong. This indicates that the

natural frequency of the wave packet plays the role of selector for the frequency of its external forces, so that the ocean has the strongest resonance to the external forces with identical or similar frequencies with its natural frequency, therefore limiting the range of the period of inter annual variability of the ENSO and the IOD. Although this paper has adopted a linear ocean model and has not considered either wind stress or air-sea interaction, the spatial field and the inter annual and decadal periods of oscillation obtained in this paper are close to actual ones.

This is not to deny the importance of nonlinear interaction or the external forces (air-sea interaction included), as the former will lead to the oscillation frequencies from extremely low to extremely high frequencies in the air-sea system, while the latter is the cause for equatorial oceanic oscillation; the importance of the selector lies in the resonance of the equatorial ocean, which determines that the oscillation frequency of the equatorial ocean is its natural frequency, which is closely related to the length of the equatorial ocean but not much related to the nonlinear interaction or external forces, therefore providing physical explanations for the findings of Dong et al. (2016). The non-linear interaction, the external forces and the resonance are key factors for the ENSO and the IOD events in the equatorial ocean, among others, all of which are indispensable. The above results also indicate the actual existence of the resonance.

Finally, it is worth noting that the wave packet in the bounded equatorial ocean in this paper does exist in the actual ocean. This wave packet is the superposition of eastward travelling Kelvin waves and westward travelling Rossby waves with the slowest speed, which satisfies boundary conditions. Therefore, the function and effect of these two waves must receive sufficient attention in physical oceanography.

5 Conclusions

This paper uses linearized shallow water perturbation equations with approximation in equatorial β plane, and introduces a reduced gravity to obtain the analytical solution of the wave packet anomalies on the upper bounded equatorial ocean. The calculation results are given and compared with flow field anomalies in the tropical Pacific Ocean and the tropical Indian Ocean, thus answering the questions raised in the introduction of this paper. The main conclusions are as follows.

(1) The wave packet is the superposition of eastward travelling Kelvin waves and westward travelling Rossby waves with the slowest speed, and satisfies the boundary conditions of eastern and western coasts respectively. The configuration of the flow field and thickness anomalies correspond to positive and negative thickness field perturbations in east-west zonal flows, which is consistent with the classic equatorial Kelvin wave.

(2) The coefficient determining the degree of attenuation of the wave packet to the north and south sides of the equator is inversely proportional only to the square root of the product of the reduced gravity and the mean depth of the upper water, which means it is inversely proportional to the phase velocity of Kelvin waves in the upper waters. The wave packet has the same speed of decay when the phase velocity is fixed.

(3) The oscillation frequency of the wave packet is proportional to its mode number l and the above phase velocity of Kelvin wave and is inversely proportional to the length of the equatorial ocean in the east-west direction. This oscillation frequency is the natural frequency of the ocean. Smaller mode number of the solution, lower phase velocity and longer length correspond to lower frequency and longer oscillation period; the oscillation period is the longest in Mode 1 of the solution.

(4) The flow anomalies of the wave packet of Mode 1 appear as zonal flows with the same direction most of the time, reach the maximum at the center of the equatorial ocean and decay rapidly away from the equator in the form of equatorially trapped waves.

(5) The flow anomalies of the wave packet of Mode 2 appear as zonal flows with the same direction most of the time in half of the ocean, and are always 0 at the center of the entire ocean, indicating stagnation. The flow anomalies decay to the north and south sides of the equator with the same speed as that of Mode 1.

(6) The spatial structure and oscillation period of the wave packet solution of Modes 1 and 2 are consistent with the changing periods of the surface spatial field and time coefficient of the first and second modes of the complex EOF analysis of the flow anomalies in the actual equatorial ocean. This indicates that the solution does exist in the actual ocean, and that the ENSO and the IOD are both related to Mode 2.

(7) The length of the bounded equatorial ocean is the sum of that of the tropical Indian Ocean and the tropical Pacific Ocean, so that this wave packet can explain the decadal variability (about 20 a) of the equatorial Pacific and the equatorial Indian Ocean after considering the Indonesian throughflow.

It is worth noting that, as this is a theoretical investigation, the model is simplified where necessary, (considering the east and west coasts in the North-South direction, etc.) leading to certain differences from the actual situations. It is therefore natural and understandable that our results differ slightly from those obtained through the complex EOF analysis of the actual ocean despite overall consistency.

References

Chao Jiping. 1993. Ensodynamics (in Chinese). Beijing: Meteorological Press, 70–90

Dong Lu, Zhou Tianjun, Dai Aiguo, et al. 2016. The footprint of the inter-decadal pacific oscillation in Indian Ocean sea surface temperatures. Scientific Reports, 6: 21251, doi: 10.1038/srep21251

Hirst A C. 1989. Slow instabilities in tropical ocean basin-global atmosphere models. Journal of Atmospheric Sciences, 45(5): 830–852

Houghton R W, Tourre Y M. 1992. Characteristics of low-frequency sea surface temperature fluctuations in the tropical Atlantic. Journal of Climate, 5(7): 765–772, doi: 10.1175/1520-0442(1992)005<0765:COLFSS>2.0.CO;2

Keller K M, Joos F, Lehner F, et al. 2015. Detecting changes in marine responses to ENSO from 850 to 2100 C.E.: insights from the ocean carbon cycle. Geophysical Research Letters, 42(2): 518–525, doi: 10.1002/2014GL062398

Lu Xu, Bao Yun, Lv Qingping. 2014. CEOF analysis for upper current of tropic Pacific Ocean. Marine Forecasts (in Chinese) , 31(2): 56–66

Lu Xu, Zhang Yongpeng. 2009. Dynamic statistics and diagnostic analysis for air-sea integrated system in the tropical Pacific Ocean in May. Advances in Marine Science (in Chinese), 27(4): 411–420

Matsuno T. 1966. Quasi-geostrophic motions in the equatorial area. Journal of the Meteorological Society of Japan, 44(1): 25–42, doi: 10.2151/jmsj1965.44.1_25

Sein Z M M, Ogwang B A, Ongoma V, et al. 2015. Inter-annual variability of summer monsoon rainfall over Myanmar in relation to IOD znd ENSO. Journal of Environmental & Agricultural Sciences, 4: 28–36

Su Tonghua, Xue Feng, Sun Hongchuan, et al. 2015. The El Niño-Southern Oscillation cycle simulated by the climate system model of Chinese Academy of Sciences. Acta Oceanologica Sinica, 34(1): 55–65, doi: 10.1007/s13131-015-0596-9

Sun Shuangwen, Fang Yue, Tana, et al. 2014. Dynamical mechanisms for asymmetric SSTA patterns associated with some Indi-

an Ocean dipoles. Journal of Geophysical Research, 119(5): 3076–3097

Wu Rongsheng. 2002. Atmospheric Dynamics (in Chinese). Beijing: China Higher Education Press, 256–269

Xuan Lili, Qiu Yun, Xu Jindian, et al. 2014. Seasonal variation of surface-layer circulation in the eastern tropical Indian Ocean. Journal of Tropical Oceanography (in Chinese), 33(1): 26–35

Yamagata T, Masumoto Y. 1989. A simple ocean-atmosphere coupled model for the origin of a warm El Niño Southern Oscillation event. Philosophical Transactions of the Royal Society A, 329(1604): 225–236, doi: 10.1098/rsta.1989.0072

Yan Xiaoyong, Zhang Ming. 2004. A study of the Indian Ocean dipole influence on climate variations over East Asian monsoon region. Climatic and Environmental Research (in Chinese), 9(3): 435–444

Zhang Ming. 1995. A study of the unstability in the barotropic vortex. Scientia Atmospherica Sinica (in Chinese), 19(6): 677–686

Zhang Dongling. 2006. Dynamic statistic analysis of space structure and time evolution in Asian summer monsoon (in Chinese) [dissertation]. Beijing: Institute of Atmospheric Physics Chinese Academy of Sciences

Zhang Dongling, He Juanxiong. 2005. Dynamic statistic diagnosis of upper current in tropical Indian Ocean. Climatic and Environmental Research (in Chinese), 10(3): 387–400

Zhang Ming, Zhang Lifeng. 2006. Wave spectra analysis in spherical barotropic atmosphere. Journal of Hydrodynamics , 21(1): 130–138